Check for updates

View Article Online
View Journal

Chemical Science

Accepted Manuscript

This article can be cited before page numbers have been issued, to do this please use: M. Su, J. Yang, W. Yang, Z. Ye, R. Wang, J. Qin, D. Song, R. Yuan, P. Ma, Y. Zhuo, C. Yang and W. Liang, *Chem. Sci.*, 2026, DOI: 10.1039/D6SC03635J.

This is an Accepted Manuscript, which has been through the Royal Society of Chemistry peer review process and has been accepted for publication.

Accepted Manuscripts are published online shortly after acceptance, before technical editing, formatting and proof reading. Using this free service, authors can make their results available to the community, in citable form, before we publish the edited article. We will replace this Accepted Manuscript with the edited and formatted Advance Article as soon as it is available.

You can find more information about Accepted Manuscripts in the Information for Authors.

Please note that technical editing may introduce minor changes to the text and/or graphics, which may alter content. The journal's standard Terms & Conditions and the Ethical guidelines still apply. In no event shall the Royal Society of Chemistry be held responsible for any errors or omissions in this Accepted Manuscript or any consequences arising from the use of any information it contains.

ROYAL SOCIETY OF CHEMISTRY

rsc.li/chemical-science

View Article Online
DOI: 10.1039/D6SC03635J

ARTICLE

Cyclic transformation of stable/metastable nucleic acid structures enables dynamic monitoring of ATP in living cells

Received 00th January 20xx,
Accepted 00th January 20xx

DOI: /x0xx00000x

Ming-Li Su[a, #], Jun Yang[a, #], Wei-Guo Yang[a, #], Zhuo-Xin Ye[c], Rui-Wen Wang[a], Jia-Min Qin[a], Da-Qian Song[c], Ruo Yuan[a], Pin-Yi Ma[c], Ying Zhuo[a], ChaoYong Yang[b], Wen-Bin Liang[a, *]

The maintenance of living systems relies on complex signaling networks involving nucleic acids, proteins and small molecules. However, conventional analytical approaches are often limited to endpoint measurements or analyses performed outside native biological environments, restricting the ability to monitor biomolecular dynamics in space and time. Here we report an artificial riboswitch-based dynamic sensing system that enables programmable nucleic acid regulation through metastable equilibrium fluctuations and steady-state conformational transitions. Through specific molecular recognition and environmental stimulation, this system enables real-time monitoring of small-molecule distributions within complex intracellular environments. Using ATP as a representative target, the platform exhibits dynamic fluorescence responses with mitochondria-associated localization and temporal fluctuation patterns in living cells. This artificial riboswitch strategy provides a versatile platform for programmable nucleic acid dynamic sensing and offers a potential approach for investigating the spatiotemporal behaviors of biomolecules in living systems.

Introduction

Life systems are orchestrated through dynamic biological equilibrium networks composed of proteins, nucleotides and small molecules that cooperatively regulate cellular functions. In these dynamic biological networks, small molecules perform dual functional roles as building blocks of biomacromolecules and regulators of the dynamic equilibrium reactions[1]. While recent single-molecule analytical technologies have achieved unprecedented sensitivity in quantifying small biological molecules like adenosine triphosphate (ATP)[2,3], nicotinamide adenine dinucleotide (NADH), performing a feat that was previously unattainable, conventional technologies, such as chromatography and mass spectrometry involving disruptive samples detached from living systems, as well as in situ fluorescence imaging relying on irreversible nucleic acid amplification systems, are still constrained by the phenomenon of static "dead data" due to their disruptive sampling protocols[4,5]. This fundamental limitation obstructs the four-dimensional dynamic concentration and spatiotemporal localization of biomolecules, which is a critical requirement for elucidating functional mechanisms in living systems. Our recent development of a dynamic analysis strategy based on sequence-structure bispecific RNA with state-adjustable molecules enables to track the dynamic concentration and spatiotemporal localization of microRNA in live cells[6]. This strategy revealed functional correlations between intracellular microRNA dynamics and cellular viability and apoptosis, providing a new approach for dynamically monitoring intracellular biomolecules. Notwithstanding these advances in the investigation of biological functions in cell with microRNA, extending such dynamic analysis strategy to small biological molecules remains an unresolved challenge due to the inherent complexity of small molecule interactions within live systems, particularly in achieving dynamic analysis modalities compatible with native cellular environments in live cells.

In living systems, organisms have evolved special ligand-responsive nucleic acid motifs, termed as riboswitches[7–9], to sense biological molecules including small molecules through ligand-responsive conformational switching. These structured nucleic acids exhibit highly specific ligand-recognition capabilities and undergo programmable conformational transformations upon target binding. This conformational flexibility enables riboswitches to respond reversibly to environmental stimuli within living systems, transducing molecular signals into regulatory outputs and highlighting their critical role in molecular regulation. While engineered aptamers have greatly advanced bioanalytical applications, the SELEX process primarily focuses on isolating aptamers with high binding affinity while providing limited insight into detailed structure–activity relationships[10,11], especially the conformational dynamics during molecular interactions[12]. Although significant methodological advances have reduced the experimental burden associated with traditional SELEX, most approaches remain focused on endpoint affinity characterization rather than capturing dynamic structural transitions. More recently, the rational design of artificial ribonucleotides has increasingly benefited from the integration of

[a] Key Laboratory of Luminescence Analysis and Molecular Sensing (Southwest University), Ministry of Education, Institute of Developmental Biology and Regenerative Medicine, College of Chemistry and Chemical Engineering, Southwest University, Chongqing 400715, P. R. China. E-mail: wenbinliangasu@gmail.com.
[b] Institute of Molecular Medicine, Shanghai Key Laboratory for Nucleic Acid Chemistry and Nanomedicine, State Key Laboratory of Oncogenes and Related Genes, School of Medicine, Shanghai Jiao Tong University, Shanghai, 200127, China.
[c] College of Chemistry, Jilin Province Research Center for Engineering and Technology of Spectral Analytical Instruments, Jilin University, Changchun, 130012, China.

Open Access Article. Published on 02 June 2026. Downloaded on 6/3/2026 5:39:44 AM.
This article is licensed under a Creative Commons Attribution-NonCommercial 3.0 Unported Licence.

Chemical Science Accepted Manuscript

View Article Online
DOI: 10.1039/D6SC03635I

SELEX and computational modelling, providing thermodynamic insights and valuable guidance for aptamer engineering[13]. Indeed, recent studies have begun to uncover these mechanistic aspects, contributing to a more comprehensive understanding of aptamer–ligand recognition and paving the way for more transparent and rational SELEX strategies. In addition, although most existing aptamer-recognition-based nucleic acid amplification reactions have achieved highly sensitive analysis of various targets, these methods are almost exclusively dependent on toehold-mediated strand displacement reactions. It has been demonstrated that a toehold length of at least 3 nt is required to provide sufficient thermodynamic driving force for efficient strand displacement and sensitive detection.[14–16]. While riboswitch paradigms indicate the potential for monitoring the dynamic concentration and spatiotemporal localization of small biological molecules in live cells, the most important fundamental knowledge gap that impeded this progress is the incomplete understanding of the small molecule-aptamer interaction and the thermodynamic changes during small molecule-induced nucleic acid conformational transitions that has become an obstacle to the construction of artificial nucleic acid reaction and equilibrium networks in cells through the functional design of aptamers[17–19]. Addressing this knowledge gap will facilitate the design of novel systems for monitoring the dynamic distribution of small molecules within complex biological networks that underpin life processes[20]. Obviously, establishing such foundational knowledge through investigations of the interaction mechanisms and thermodynamic changes between small molecules and aptamers will enable the engineering of artificial riboswitches for programmable dynamic responses to small molecules. This capability represents a critical step toward elucidating the dynamic distribution of small molecules within the intricate biological networks that drive life processes[21,22].

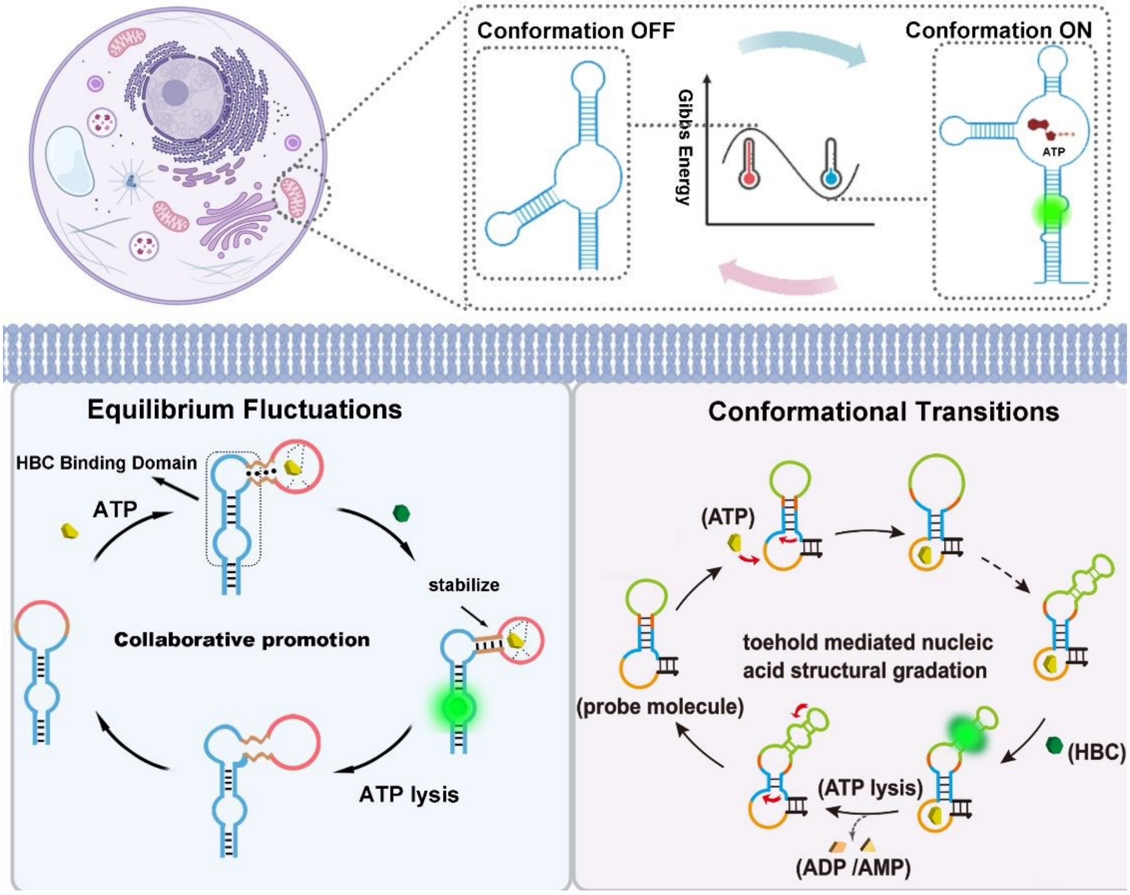

Fig. 1 Scheme of Nucleic Acid Stable/Metastable Structure Cyclic Transformation Enable Spatiotemporal Monitoring of Small Molecule in Living Cells.

To address the challenges of demonstrating dynamic four-dimensional distribution of small molecules in living systems by resolving small molecule-aptamer interactions and monitoring subtle thermodynamic changes during target-triggered conformational switching for their potential applications, herein, using ATP[23,24] and NADH (Fig. S1) as model ligands, we programmed the aptamer principles via in silico molecular docking simulations and systematically demonstrated the main interactions between the model small molecules and their aptamers, identifying critical recognition mechanism mediated by hydrogen bonds and π-π interactions[25–27]. Departing from conventional unidirectional reactions based on aptamer–complementary strand interactions, we engineered a functionalized single-chain aptamer as a unimolecular artificial riboswitch driven by multi-ligand-responsive structural transitions. This strategy exploits the nucleic acid binding funnel and free-energy landscape, where ligand–nucleic acid interactions can generally be described by “equilibrium fluctuations” and “conformational transitions” associated with the cyclic

Open Access Article. Published on 02 June 2026. Downloaded on 6/3/2026 5:39:44 AM.
This article is licensed under a Creative Commons Attribution-NonCommercial 3.0 Unported Licence.
Chemical Science Accepted Manuscript

Please do not adjust margins

View Article Online
DOI: 10.1039/D5SC08351J

Open Access Article. Published on 02 June 2026. Downloaded on 6/3/2026 5:39:44 AM.
This article is licensed under a Creative Commons Attribution-NonCommercial 3.0 Unported Licence.

Chemical Science Accepted Manuscript

interconversion between stable and metastable nucleic acid structures, respectively (Fig. 1). By incorporating these energy landscape features into a self-regulated artificial riboswitch, we established a real-time dynamic tracking platform for monitoring the spatiotemporal redistribution and concentration changes of target small molecules through the dynamic equilibrium between metastable nucleic acid structures regulated by the target molecules and stable structures modulated via multistage strand displacement processes triggered by the targets[28]. This strategy enables continuous monitoring of the dynamic distribution of small molecules within living systems through cyclic transformations between stable and metastable nucleic acid structures, providing a new tool for understanding the behaviours of small molecules in complex biological networks.

Results and Discussion

Mechanisms of Nucleic Acid Conformational Transitions

Beyond their canonical genetic functions in living organisms, RNA molecules possess intrinsic conformational switching capabilities involved in the regulation of epigenetic processes. Riboswitches exemplify this phenomenon by functioning as biological logic gates that coordinate signalling networks through ligand-responsive nucleic acid conformational transitions. They exhibit remarkable efficacy based on the dynamic conformational regulations of nucleic acids in promoting signal transduction of various molecular processes, including small molecule-nucleic acid, protein-nucleic acid and inter-nucleic acid interactions, enabling precise spatiotemporal control over cellular processes[29]. Our foundational models (Fig. 2) demonstrate how sequence-encoded thermodynamics govern nucleic acid structural conformation switching by regulating the reaction constants among different nucleic acid conformations *via* adjusting the bases of the nucleic acid bases[30]. As illustrated in Fig. 2A, two dominant conformations, designated as *C*s1 and *C*s2, coexist with a population ratio of $\boldsymbol{k_1} = \frac{c_{s2}}{c_{s1}}$ dictated by ΔG[31], which could be regulated *via* the stem in the complementary middle region of *C*s1. As calculated based on the RNAfold system, the stem is in an unpaired open state with a free energy of -26.44 kcal/mol due to interference from factors such as ring tension and electrostatic forces (Fig. S2). Compared with the short stem fully base-paired conformation *C*s2, its free energy is -24.3 kcal/mol. The reaction coefficient *k* between these two conformations could be calculated as 0.12, which shows that under natural conditions, *C*s1 is the dominant conformation. When $\boldsymbol{k_1}$ is of a considerable magnitude, it signifies that the concentration of *C*s2 is markedly elevated in comparison to *C*s1, thereby indicating that the *C*s2 conformation constitutes the predominant component within the nucleic acid system (Fig. 2G). It is noteworthy that the base can be tailored to align with the specific requirements of the intended application, thereby enabling precise regulation of $\boldsymbol{k_1}$ and facilitating adaptation to diverse scenarios. When a nucleic acid is functionalized with an aptamer and the target is introduced into the reaction system, the target assumes a conformationally balanced state within a solution that is conducive to the formation of a stable bond between the target and the aptamer. This bond is supported by intermolecular forces, including hydrogen bonds and π-π stacking, which facilitate the interaction between the target and the aptamer. In this state, there is a target recognition-induced dynamic binding equilibrium of $\boldsymbol{k_2} = \frac{c_{T-c_{s2}}}{c_T \cdot c_{s2}}$. In this state, we hypothesize that there is a significant degree of fluidity between its various conformations due to the inherent complexity and diversity of the aptamer conformations[32]. When the aptamer recognizes its target, other nucleic acid conformations with lower binding activity often shift toward those with higher activity. Although this shift is unfavourable from an entropy change perspective, the enthalpy change can offset the negative impact of entropy change. The high mobility brought about by this regulation enables the rapid adjustment of the proportion of various conformational components through the addition of targets, achieving precise regulation of multiple conformations. Calculations indicate that the binding energy between ATP and its aptamer is -9.1 kcal/mol (aptamer in equilibrium fluctuations model). This suggests that during the conformational transition, the binding of ATP to the aptamer not only drives the nucleic acid conformational change, but also stabilizes the stem region throughout the entire process. Based on these mechanisms, the rate constant of k_2=8.05 $\times$ 10^4 could be calculated that demonstrated the highly efficient conformational fluctuations regulated by target small molecules (calculation process in supporting information). However, nucleic acid conformational transformation driven by a single short stem structure shows limited plasticity with typical thermodynamic (free) energy difference (ΔG) of approximately 5 kcal/mol, and it is impossible to achieve transformation between conformations with similar energy minima but extremely different structures[33,34].

In addition to nucleic acid equilibrium fluctuations with thermodynamic barriers driven by a single short stem structure, we also engineered dynamic regulation of nucleic acid conformation by toehold-mediated strand displacement cascades of nucleic acid stable structure named as conformational transitions. Once the target recognizes the binding domain in the aptamer, it effectively competes with the nucleic acid self-folding at the outset of the binding process. This relies on a significant enthalpy-driven energy change arising from nucleic acid self-folding. The kinetic rate is relatively slow in comparison with that of ligand-induced nucleic acid equilibrium fluctuations; however, once the reaction energy barrier is reached, the nucleic acid conformation is broken[35]. At this juncture, the recognition sequence and the locking sequence in the initial nucleic acid conformation gradually dissociate. This subtle change in the recognition sequence is then transmitted to the entire nucleic acid, where a displacement reaction gradually occurs. This reaction induces the nucleic acid to rearrange into the required functional conformation. However, this conformation requires stabilization by the hydrogen bond formed between the ligand and nucleic acid to maintain its structure. Upon ligand dissociation, the nucleic acid lacks the requisite energy to maintain its conformation. The mediation of the toehold facilitates the nucleic acid's dissociation in a direction that is entirely opposite to that of the initial reaction, subsequently enabling its refolding back to the initial conformation. In contrast to nucleic acid conformational migration initiated by a single short stem

Please do not adjust margins

View Article Online
DOI: 10.1039/D6SC03675J

structure, nucleic acid conformational transitions with toehold-mediated strand displacement (TMSD) cascades permit the reciprocal conversion of local structures, thereby facilitating a more expeditious pathway for RNA conformational rearrangement within the challenging and intricate free energy landscape. As illustrated in Fig. 2E and Fig. S4, ATP-EF demonstrates a markedly faster kinetic signal response compared with ATP-CT. In contrast, owing to multi-level intramolecular strand displacement–driven nucleic acid conformational rearrangements, ATP-CT exhibits a substantially expanded linear dynamic range (Fig. 2).

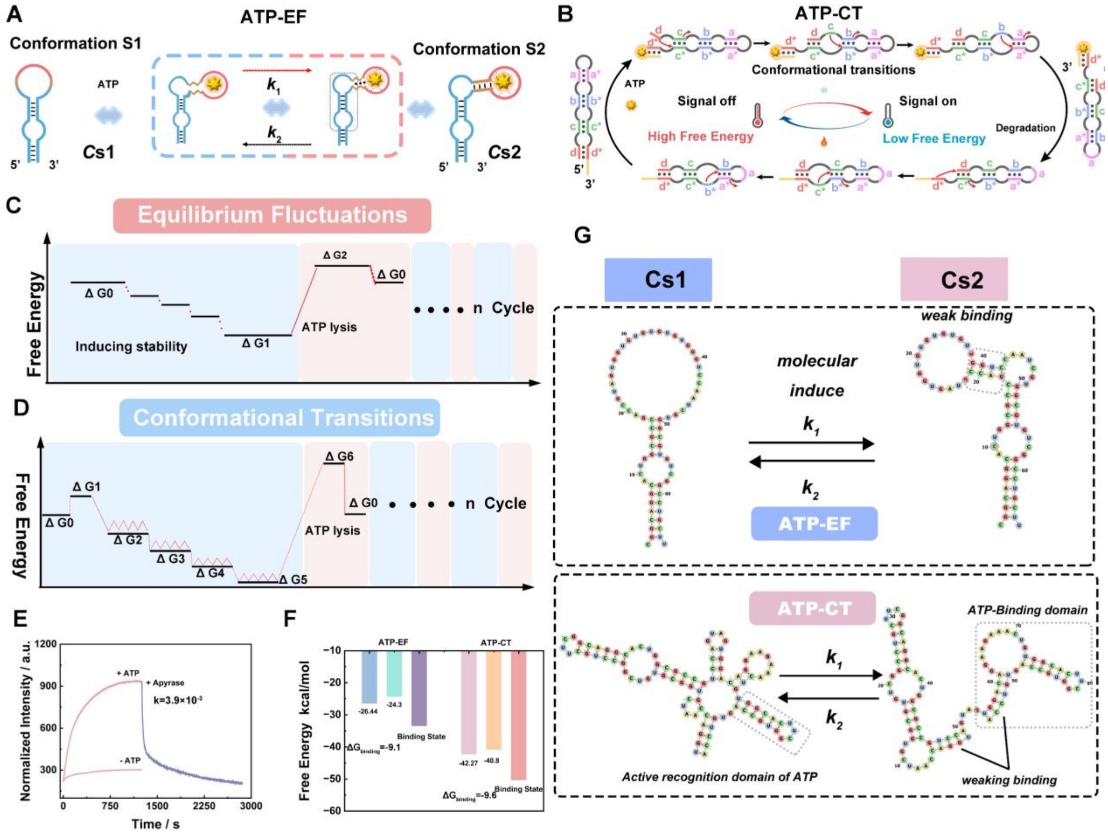

Fig. 2 Mechanism of (A) nucleic acid equilibrium fluctuations and (B) conformational transitions. The correspond free energy changes in (C) nucleic acid equilibrium fluctuations and (D) conformational transitions. (E) In vitro fluorescence kinetic test of ATP concentration (5 mM) regulation, (F) free energy of each conformation. (G) Detailed illustration of the nucleic acid conformational transformation process induced by ATP binding, showing sequential base-pair rearrangement, stem dissociation, loop reconstruction, and exposure of the hidden functional domain during structural switching.

Thermodynamic Analysis of Nucleic Acid Structural Transformation Process

The generation of equilibrium fluctuations can be understood as a cellular cue (such as a change in the abundance of a specific biomarker) causing different conformations of nucleic acids to produce a non-equilibrium state, which then relaxes to the initial equilibrium state after the target dissociates. Free energy landscapes reveal RNA structural plasticity in RNA dynamics analysis as a means of better understanding RNA conformational free energy. Due to the degeneracy of base pairing and stacking interactions, double-stranded RNA is highly stable in a deep local minimum in the free energy landscape, which means that under the intervention of ring tension, there is a kinetic barrier to the conversion to this conformation. The energetically favourable RNA conformation allows RNA to undergo great structural transformation. Once the ligand binds to the RNA, a large number of nucleic acids in this conformation will be guided to a specific set of conformations. The binding of small molecules to RNA is more enthalpy-driven. Small molecules regulate the nucleic acid landscape by changing RNA conformation, thereby modulating RNA function. Taking the equilibrium fluctuation type as an example, when RNA conformational transformation does not involve too much dissociation or rearrangement of paired bases, the enthalpy change while the binding of small molecules to RNA is sufficient to drive the transfer of nucleic acid conformation, which means that the free energy is similar in the free energy landscape, but in fact there is a certain kinetic barrier, and an induction factor is required to achieve conformational transformation. In the context of metastable nucleic acid conformational regulation, the system operates at the critical point of nucleic acid conformational change, where only a small perturbation is required to trigger conformational migration. Unlike the multi-level cascade transitions observed in stable nucleic acid structures, this regulatory mechanism resembles the movement of chemical equilibria. Initially, the signal module and the recognition module are connected by a short base pair. Due to ring strain, this short base pair cannot effectively stabilize the signal domain in the absence of the target molecule. In the absence of the target, the free energy of the system is at G_0. Upon binding of the target molecule to

Open Access Article. Published on 02 June 2026. Downloaded on 6/3/2026 5:39:44 AM.
This article is licensed under a Creative Commons Attribution-NonCommercial 3.0 Unported Licence.
Chemical Science Accepted Manuscript

Please do not adjust margins

View Article Online
DOI: 10.1039/D5SC03631J
Open Access Article. Published on 02 June 2026. Downloaded on 6/3/2026 5:39:44 AM.
This article is licensed under a Creative Commons Attribution-NonCommercial 3.0 Unported Licence.
Chemical Science Accepted Manuscript

the recognition module, the binding stabilizes the structure, leading the connecting sequence to progressively bind, thereby lowering the conformational free energy to G_1. When the target dissociates, the weak base-pairing interaction between the connecting stem and the recognition module no longer supports the stem's position, causing it to dissociate and return to the G_0 state.

The small molecule-driven cascade nucleic acid conformational rearrangement involves transitions between the two RNA conformations separated by overcoming substantial free energy barriers. While small molecule binding disrupts local RNA structures with one or two base pairs, these cooperative perturbations guide the RNA into a distinct three-dimensional structure *via* programmable base-editing. This transformation traverses the intermediate energy minima within the free energy landscape, which was driven by ligand-binding enthalpy that initiates localized structural destabilization. Subsequent ligand degradation reverses the process, restoring native conformations through hydrogen bond dissociation. As shown in Fig. 2B, the toehold-mediated strand displacement–driven cascade transition involves multiple transition-inducing structures, which is initially locked with only the active recognition of aptamer module. The detailed nucleic acid rearrangement pathway during this cascade process is illustrated in Fig. S5. The complementary module G_0 state with multi-locked sequence and the recognition sequence of the aptamer. When the target molecule binds to the recognition module, the free energy of the system briefly increases to G_1, due to ambient ionic strength effects, and then, the stronger binding energy induces *a* conformational transformation in the nucleic acid, displacing the *d* sequence paired with the *d** sequence. The weak interaction between the bases *c* and *c** is insufficient to stably maintain the conformation, leading to their gradual dissociation. Simultaneously, the dual forces of free energy and the hybridization potential of the free *d* and *c** bases drive the displaced *d* sequence to attack *c**, forming a more stable intermediate conformation. The sequences *a*, *b*, *c*, and *d* exhibit more sequence similarity and high editability, which is in a locked state with G_0 state *via* weak base-pairing energies. Once the initial structural trigger occurs, a domino-type cascade transition of the nucleic acid structure is initiated. Specifically, *c* can attack the recently dissociated *b** sequence, displacing *b*, which then attacks *a**, ultimately completing the structural rearrangement. This process realizes the small molecule-induced nucleic acid conformational transformation. Upon degradation of the small molecules, the system's freedom increases rapidly, exposing the locked *d** as the initiator for the reverse transition. Driven by free energy, this initiates the reverse cascade transition, culminating in the structural rearrangement of the nucleic acid. In the absence of ATP, the nucleic acid adopts a locked conformation with a free energy of -42.27 kcal/mol. Upon ATP binding, computational analysis reveals a docking energy of -9.6 kcal/mol between ATP and the nucleic acid (aptamer in conformation transition model). Additionally, π–π stacking interactions between the adenosine moiety of ATP and the aromatic nucleobases within the aptamer further stabilize the complex. The resulting binding energy not only reinforces the nucleic acid conformation but also drives a stepwise conformational transition process. Notably, the calculated reaction constant ($k = 5.45 \times 10^5$) indicates a substantially more complete conformational transformation compared with transient fluctuations within the equilibrium state.

Mechanisms of Molecular Binding.

Based on computational analyses of the ATP and the tertiary binding states of small molecules with nucleic acids, the binding domains of HBC and ATP are entirely distinct and exhibit no tertiary folding interactions, such as those observed in pseudoknots[36–38]. The binding probe of nucleic acid is relatively complex (Fig. 3A and 3B), with three stems P1 (gray), P2 (purple red), and P3 (khaki), two internal loops J3/2 (orange yellow) and J2/1 (blue), and one terminal loop L1 (green). Among them, J3/2 forms an inner fold and is continuously stacked with P1, J2/1, and P2 to form a stable double helix structure. Notably, L1, which constitutes the binding domain of ATP, is independent of the remaining regions and adopts a helical conformation. With the exception of the terminal base that has undergone a change in orientation, the internal conformation of the remaining bases exhibits a range of sugar puckering and base flips.

The helical L1 domain of ATP-equilibrium fluctuation (ATP-EF) forms a binding pocket between the two fragments of continuous nucleosides 23U-24A-25G and 29U-30G-31U-32G-33U, which provides a binding spatial environment for interactions between ATP and ATP-EF. Among them, 23U, 27G, 34G, and 35U serve as the boundary bases of the binding pocket, enabling high-affinity ATP recognition mainly based on intermolecular hydrogen bonding and π-π stacking. Typically, 27G forms 1H bond with γ-PO_4^{3-}, and the glycoside of 23U adopts a wrinkled conformation to form 1H bond with α-PO_4^{3-}. The hydrogen bonding between these nucleic acids and the phosphate group of ATP contributes to in specific recognition of ATP molecules, especially in the recognition of aptamers to structural analogs such as AMP and ADP (Fig. S6, S7). Additionally, the hydroxyl groups on the glycoside form 4H bonds with 34G and 35U that promotes the stability of the nucleic acid conformation. The base of 23U shows a similar inclination to adenosine A, tends to be parallel in space, and resulting in π–π stacking interactions. A binding energy of -9.1 kcal/mol between ATP and ATP-EF was obtained using AutoDock Vina. The steady-state nucleic acid conformational transformations were analyzed based on the molecular docking experiments also with nucleic acid tertiary structure. ATP-conformational transitions (ATP-CT) exhibits higher structural complexity than ATP-EF with ATP binding region mediated by the loop L1 (brown) and internal loop J2/1 (red) interconnected by stems P1 (green) and P2 (gray). The L1 and P1 domains adopt bent conformations rather than a simple double helix rise, forming a stable binding pocket of ATP. The nucleic acid structure was undergoes pronounced structural rearrangement at 70C-71U-72G, while J2/1 as an internal loop with loose structure. On the contrary, the loop structure also exhibits partial inward helical contraction. As illustrated in Fig. 3A, the bases 57G, 58G, and 62G stack above ATP, while 63G, 64A, 68A, and 69A form a lower stacking layer, forming a sandwich-like recognition interface through cooperative stacking interactions. These bases interact with the base, pentose, and phosphate groups of ATP, respectively, thereby constructing a stable spatial binding domain that ensures the stable binding of ATP as a ligand to ATP-CT. Similarly, the binding of the receptor and ATP is still

Please do not adjust margins

View Article Online
DOI: 10.1039/D6SC03635J

Open Access Article. Published on 02 June 2026. Downloaded on 6/3/2026 5:39:44 AM.
This article is licensed under a Creative Commons Attribution-NonCommercial 3.0 Unported Licence.

predominantly governed by hydrogen bonds and π-π stacking, akin to the binding mode observed in ATP-EF. The binding of 68A, 69A to the N atom in A base of ATP results in the formation of two hydrogen bonds. Similarly, 57G and 58G binds to the hydrogen of the amine group in A base by two hydrogen bonds. Additionally, 70C and 71U interact with A base *via* π-π stacking, forming multiple interactions with ATP and thereby ensuring the stable binding of ATP.

Isothermal titration calorimetry (ITC) is one of the state-of-the-art biotechnologies to quantitatively characterize the binding behavior between the ligand and its aptamer. The results revealed that the dissociation constant (Kd) for ATP binding was 128 nM, which is markedly lower than those for ADP (5.75 μM) and AMP (7.30 μM), corresponding to approximately 45-fold and 57-fold higher binding affinity, respectively. Consistent with these thermodynamic observations, molecular docking analyses (Fig. 3) suggest that, from both structural and energetic perspectives, ATP, owing to its complete triphosphate tail can establish multiple spatially distributed initial interactions with the aptamer, which cooperatively trigger conformational rearrangement of the nucleic acid. In addition, the larger molecular size and greater conformational flexibility of ATP facilitate its stable accommodation within the aptamer binding pocket, ultimately resulting in a high-affinity binding state. In contrast, ADP and AMP, which lack the full triphosphate moiety, exhibit intrinsic deficiencies in spatial reach, and conformational driving capability, rendering them incapable of effectively inducing cooperative structural rearrangements of the aptamer and leading only to weak and transient binding states. Furthermore, as shown in Fig. 3F, ATP binding to the aptamer is predominantly enthalpy-driven, in contrast to the lower binding affinity of ADP and AMP to this aptamer.

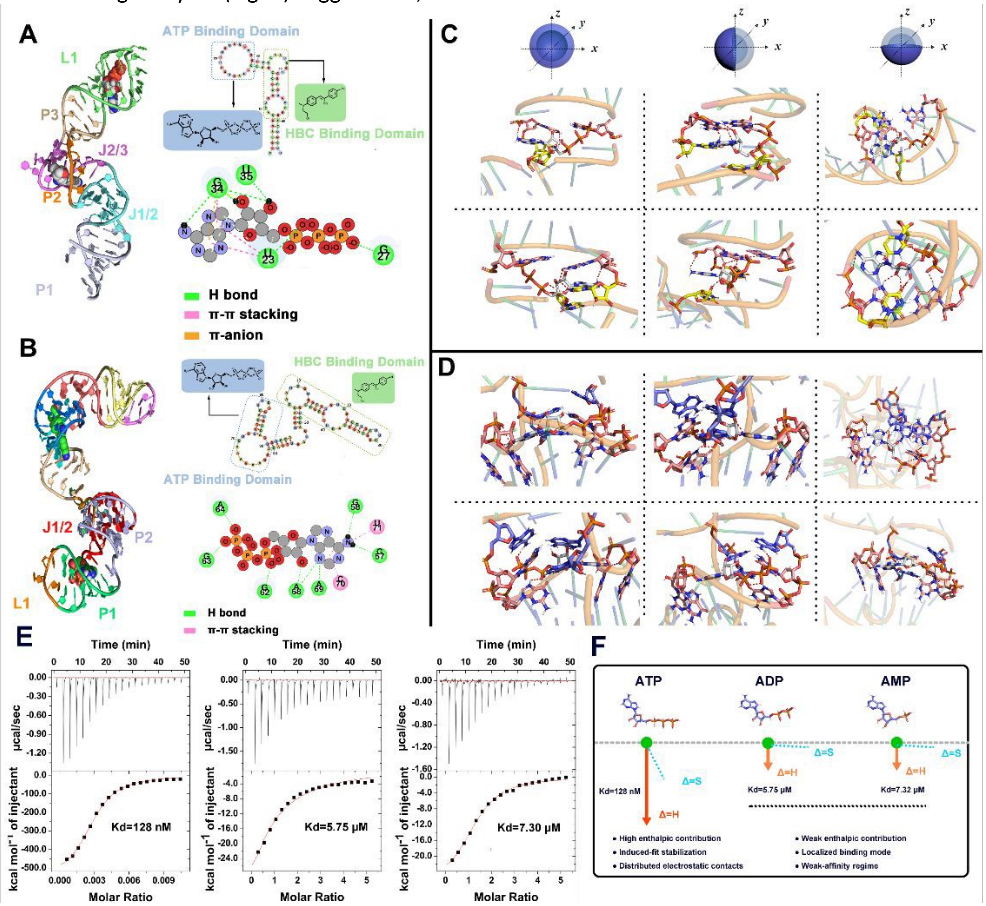

Fig. 3 Schematic diagram of the 2D docking of ATP-EF (A), ATP-CT (B) with ATP and the prediction of the 3D structure of nucleic acid. (C, D) 3D docking multi-angle display diagram. In the docking results display, green represents hydrogen bonding and pink represents π-π stacking. (E) ITC analysis of the interactions between the ATP aptamer and ATP (Kd=128 nM), ADP (Kd=5.75 μM), and AMP (Kd=7.30 μM). (F) Schematic illustration of the thermodynamic mechanisms underlying aptamer binding to ATP, ADP, and AMP

Chemical Science Accepted Manuscript

This journal is © The Royal Society of Chemistry 20xx

Please do not adjust margins

View Article Online
DOI: 10.1039/D6SC03635J

Open Access Article. Published on 02 June 2026. Downloaded on 6/3/2026 5:39:44 AM.
This article is licensed under a Creative Commons Attribution-NonCommercial 3.0 Unported Licence.

Dynamic analysis applications.

The feasibility of equilibrium fluctuation and conformational transformation driven nucleic acid structural regulation was systematically validated through computational simulations. Using ATP as a representative model target, we subsequently constructed a dynamic biosensing platform governed by multimodal conformational transitions. Key experimental parameters associated with equilibrium fluctuation-mediated nucleic acid regulation, including hybridization time (Fig. S8) and HBC concentration (Fig. S9), were comprehensively optimized to achieve enhanced sensing performance.

The buffer system was systematically optimized by comparing HEPES and TE buffers. A significantly higher signal-to-noise ratio (SNR) was obtained in HEPES buffer. In contrast, the high concentration of EDTA in TE buffer was found to interfere with the availability of metal ions in the solution, thereby affecting the stability of the nucleic acid structure. Furthermore, HEPES buffer was demonstrated to exhibits a greater buffering capacity compared to TE buffer, providing a more stable environment for nucleic acids and minimizing the impact of environmental fluctuations on nucleic acid conformation (Fig. S3). Mg^{2+} plays an indispensable role in maintaining the stability of nucleic acid structures. The concentration of Mg^{2+} directly influences nucleic acid conformation, particularly in equilibrium fluctuation-based allosteric models, which are highly responsive to environmental changes. In the case of ATP-EF, when the Mg^{2+} concentration is excessively high (Fig. S10), Mg^{2+} promotes the nucleic acid structure to transition into the Cs2 state, forming a HBC-binding domain. This transition leads to undesired signal leakage, thereby compromising SNR during analysis. Conversely, at low Mg^{2+} concentrations, the insufficient ionic strength impedes the proper folding of nucleic acids. The optimal SNR was achieved at an Mg^{2+} concentration of 5 mM. Fluorescence responses of ATP-EF and ATP-CT were evaluated with different concentrations of ATP revealed that the dynamic analysis strategy based on the equilibrium fluctuation model exhibited a linear response within the range of 100 µM to 100 mM (I = 0.66 log *c* - 1.1). Additionally, the molecule-mediated nucleic acid conformational transition strategy, characterized by larger conformational rearrangements, demonstrated an extended analytical range of 100 fM to 1 mM (I = 0.038 log *c* + 0.45). These findings underscore the broader applicability of the conformational transformation approach for biomolecular analysis in diverse concentration ranges, demonstrating the capability of the dynamic analysis probe for intracellular analysis.

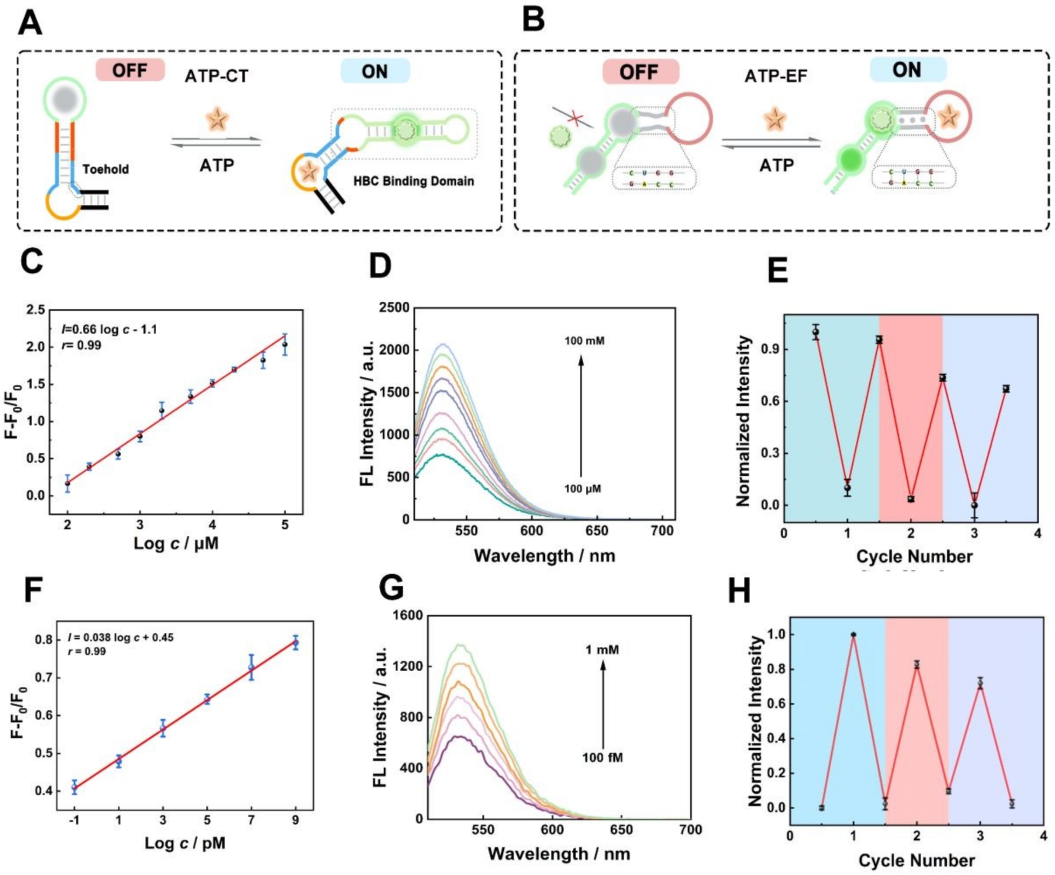

Fig. 4 (A) Conformational transitions and (B) Equilibrium fluctuation RNA signal change patterns. Calibration curve of the fluorescence intensity and the concentration of ATP with ATP-EF(C) and ATP-CT(F). Error bars: SD, n = 3, (D) The corresponding fluorescence emission spectra with different probes (D, ATP-EF, G, ATP-CT) and (E) the signal responses of multiple in vitro simulations of ATP concentration fluctuations are presented (E, ATP-EF, H, ATP-CT). Error bars: SD, n = 3.

Furthermore, we constructed an in vitro model of ATP production and consumption to repeatedly induce nucleic acid conformational transformations in order to comprehensively evaluate the feasibility of dynamic analysis for repeated ATP cycling in complex

Chemical Science Accepted Manuscript

Please do not adjust margins

View Article Online
DOI: 10.1039/D6SC03635J

Open Access Article. Published on 02 June 2026. Downloaded on 6/3/2026 5:39:44 AM.
This article is licensed under a Creative Commons Attribution-NonCommercial 3.0 Unported Licence.

intracellular environments. Apyrase-mediated ATP hydrolysis was counterbalanced by controlled ATP replenishment, inducing cyclical nucleic acid conformational switching. As can be seen in Fig. 4E and H, the fluorescence intensity in each cycle demonstrates that the small molecule dynamic analysis strategy is capable of operating in complex intracellular environments. To validate the intracellular ATP dynamic analysis capability of the designed functional molecular recognition probe, we implemented pharmacological modulation of ATP homeostasis in cells by specific drugs as ATP levels regulators[39–41]. Ca^{2+} activates Ca^{2+}-ATPase, thereby enhancing ATP metabolism and synthesis for ATP upregulation, which ultimately increases ATP levels. In contrast, oligomycin, by targeting H^+-ATPase, disrupts ATP synthesis, leading to reduced ATP levels, resulting in decreased ATP levels. As shown in Fig. 5, a 2-3 folds increase in fluorescence intensity in Ca^{2+}-treated cells and an approximately 10–20% decrease in oligomycin-treated cells in comparison with normal HeLa cells. We hypothesize that oligomycin exerts only a partial inhibitory effect on ATP synthesis. This may be due to compensatory mechanisms in cellular metabolism, such as increased glycolysis or activation of alternative phosphorylation pathways, which help maintain cellular energy levels. These results demonstrate that the two probes are capable of producing distinct signal responses to varying intracellular ATP levels, thereby enabling visualization of subcellular ATP redistribution.

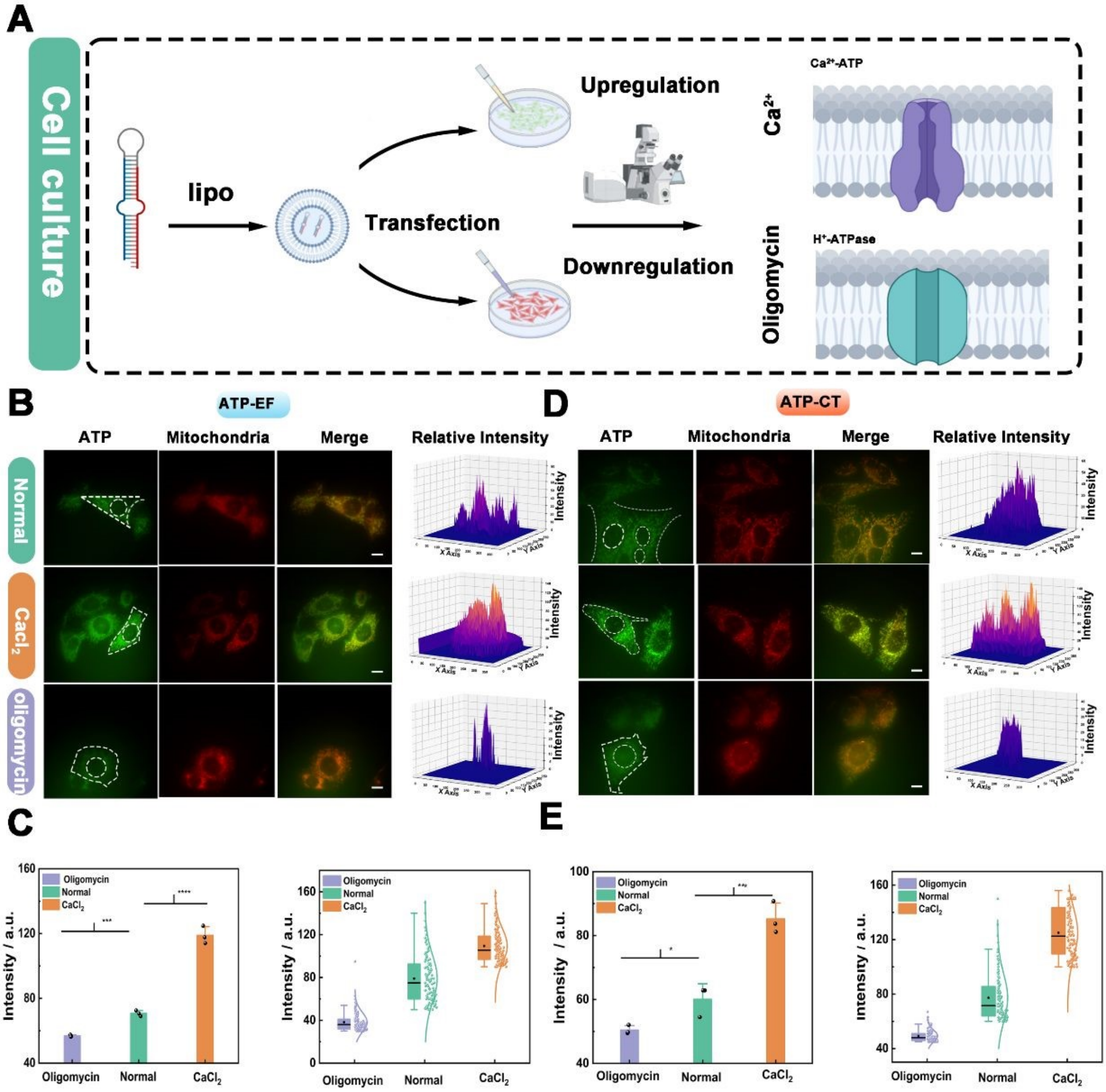

Fig. 5 (A) Schematic illustration of the cellular treatment workflow. (B) Intracellular ATP imaging using the ATP-EF probe under different drug treatments. (C) Quantitative fluorescence analysis corresponding to panel B: the C left shows the average fluorescence intensity of cells under the same treatment conditions, while the C right presents the statistical analysis of fluorescence from the imaging results. (D) Intracellular ATP imaging using the ATP-CT probe under different drug treatments. (E) Quantitative fluorescence analysis corresponding to panel D: the E left shows the average fluorescence intensity of cells under the same treatment conditions, while the E right presents the statistical analysis of fluorescence from the imaging results. Scale bar: 5 μm. (*$p < 0.05$, **$p < 0.01$, ***$p < 0.001$, and ns indicates no significant difference.)

Chemical Science Accepted Manuscript

View Article Online
DOI: 10.1039/D6SC03635J

Open Access Article. Published on 02 June 2026. Downloaded on 6/3/2026 5:39:44 AM.
This article is licensed under a Creative Commons Attribution-NonCommercial 3.0 Unported Licence.

Both dynamic analysis methods demonstrated robust ATP analysis consistent with mitochondrial colocalization. Despite extracellular validation based on these two RNA transformation models, we further evaluated the dynamic performance of the probe in a cellular setting. At different time points, significant changes in fluorescence intensity were observed in various regions of the cell, indicating that ATP within the cell undergoes active turnover. Notably, substantial ATP accumulation was observed around mitochondria, where it exhibited a radial concentration gradient (Fig. S12). As the distance from the mitochondria increases, ATP concentration gradually decreases, exhibiting a relatively lower concentration compared to the mitochondrial vicinity. Within a 20-minute observation period (Fig. 6), cellular fluorescence signals showed varying degrees of fluctuation. This further suggests that ATP, after being synthesized by mitochondria, diffuses to subcellular regions where it is required and participates in metabolic processes. Our observations reveal that the response speed of a fluctuation-based equilibrium model is faster compared to that of conformational transitions involving significant secondary structure rearrangements. This difference arises from the mode of nucleic acid conformational transformation. To rigorously exclude the possibility that the observed local fluctuations of ATP were merely artifacts introduced during the imaging process, we established a control system based on a locked aptamer sequence. In this design, the aptamer was hybridized with a BHQ1-labeled blocking strand to suppress background fluorescence. Upon specific ATP recognition, the aptamer underwent conformational rearrangement, displacing the blocking strand, leading to the separation of BHQ1 from FAM and restoration of fluorescence. This mechanism enabled real-time in situ visualization of ATP. Notably, unlike ATP-CT and ATP-EF systems that exhibited fluctuating intensity signals during imaging, the locked aptamer strategy provided highly stable fluorescence over time. These findings demonstrate not only that the observed spatiotemporal variations originate from intrinsic cellular ATP dynamics rather than random imaging noise, but also that our dynamic analysis strategy efficiently captures intracellular ATP dynamics with minimal background interference. Such robustness and efficiency highlight the potential of our approach for single-cell level dissection of ATP metabolism. Consequently, the FISHER strategy is intrinsically more applicable to endpoint characterization of the final molecular state, rather than continuous monitoring of dynamic small-molecule fluctuations. In contrast, the ATP-EF and ATP-CT strategies developed in this work are established on target-induced allosteric modulation within the nucleic acid framework, without involving irreversible strand dissociation processes. By reversibly regulating the formation and disruption of fluorophore-binding domains through conformational transitions, the system maintains temporally responsive signal transduction behaviour. This design effectively circumvents the intrinsic limitations associated with conventional strand-displacement-based imaging approaches and thereby enables dynamic monitoring of ATP fluctuations in living systems.

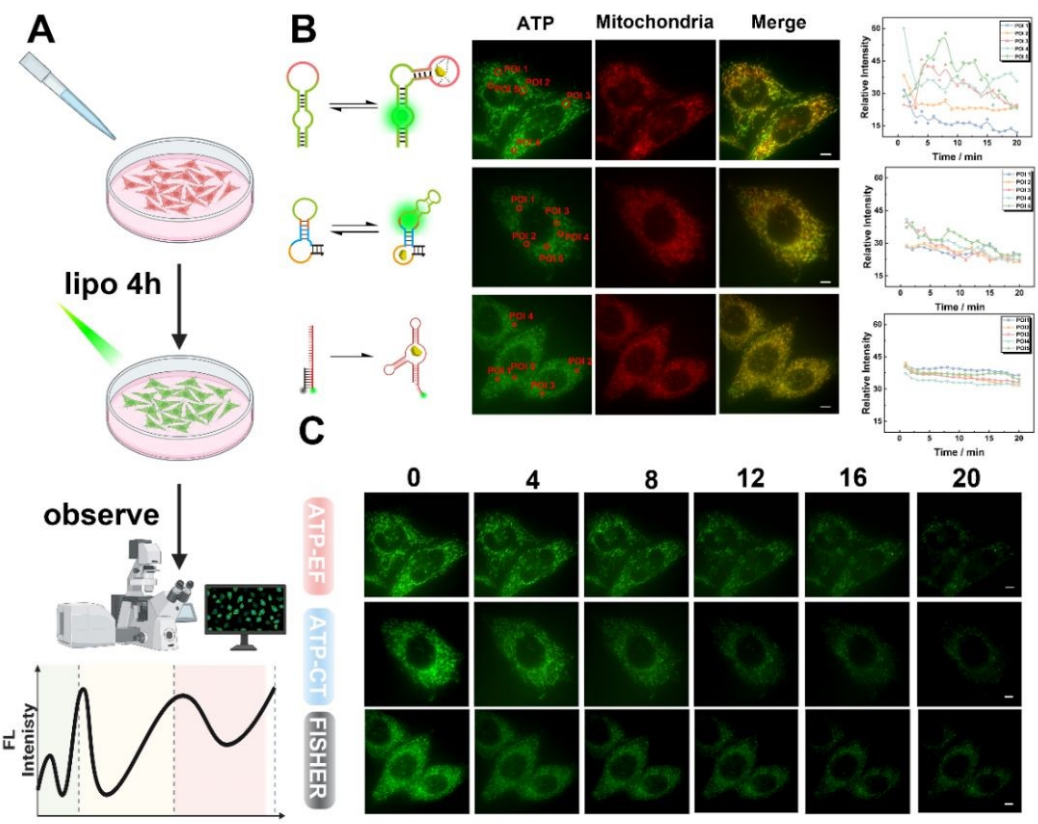

Fig. 6 (A) Schematic diagram of cell culture observation process, (B) Points of interest distributed in different areas were randomly selected, and the fluorescence intensity at different times was counted to visualize the dynamic concentration of ATP. From top to bottom they are ATP-EF, ATP-CT, FISHER (C) Confocal imaging of mitochondrial localization, and changes in cellular ATP at different times. Scale bar: 5 µm

Chemical Science Accepted Manuscript

View Article Online
DOI: 10.1039/D6SC03635J

ARTICLE

Open Access Article. Published on 02 June 2026. Downloaded on 6/3/2026 5:39:44 AM.
This article is licensed under a Creative Commons Attribution-NonCommercial 3.0 Unported Licence.

Conclusions

In conclusion, we developed an artificial riboswitch-mediated platform for biomolecular dynamic analysis based on programmable nucleic acid allosteric regulation. By integrating metastable equilibrium fluctuations and steady-state conformational transitions, the system enables target-responsive structural reconfiguration of programmable nucleic acid architectures. Through thermodynamically controlled multistage allosteric rearrangements, the nucleic acid network can return to its initial state following target degradation or metabolic turnover, enabling continuous monitoring of the spatiotemporal dynamics of small molecules in living cells. ATP was used as a representative analyte to evaluate the sensing performances of the platform, which exhibited reversible fluorescence responses, mitochondria-associated localization, and temporally resolved intracellular dynamics. Compared with conventional endpoint analytical strategies, this approach provides a dynamic and programmable framework for real-time visualization of intracellular molecular processes under physiologically relevant conditions. Collectively, this work establishes a versatile strategy for constructing nucleic-acid-based dynamic sensing systems and provides a platform for investigating intracellular biochemical regulation, molecular interaction dynamics, and metabolic behaviour in complex living systems.

Author contributions

[#]Ming-Li Su, Jun Yang and Wei-Guo Yang contributed equally to this work.

M.S. designed research; J.Y., W.Y. and Z.Y. performed research; R.W., J.Q., Z.Y., D.S., and R.Y. analysed data; W.L., Y.Z., P.M. and C.Y. supervised the work; M.S. wrote the paper.

Conflicts of interest

There are no conflicts to declare.

Data availability

All the data supporting the findings of this study are available within the article and can be obtained from the corresponding author upon reasonable request.

Acknowledgements

This work was financially supported by the National Natural Science Foundation (NNSF) of China (81972024) and Chongqing Municipal Science, Health Joint Medical Research Key Project (2025DBXM004) and Chongqing Graduate Innovation Project for Doctoral Students (CYB240101). We thank Ye Wei and Shi-Mei He (College of Chemistry and Chemical Engineering, Southwest University) for the synthesis of fluorescent dye. Some elements of the images in the article are taken from biorender.com and have obtained the necessary copyright. We would like to express our gratitude for the assistance provided by Yan Li and Lan Xu (Analytical & Testing Canter, Southwest University).

References

1 J. D. Munzar, A. Ng, M. Corrado and D. Juncker, *Chem. Sci.*, 2017, **8**, 2251–2256.
2 Q.-L. Zhang, L.-L. Wang, Y. Liu, J. Lin and L. Xu, *Nat Commun*, 2021, **12**, 4654.
3 Y. Biniuri, G.-F. Luo, M. Fadeev, V. Wulf and I. Willner, *J. Am. Chem. Soc.*, 2019, **141**, 15567–15576.
4 M. Li, F. Yin, L. Song, X. Mao, F. Li, C. Fan, X. Zuo and Q. Xia, *Chem. Rev.*, 2021, **121**, 10469–10558.
5 Y. Zhao, F. Chen, Q. Li, L. Wang and C. Fan, *Chem. Rev.*, 2015, **115**, 12491–12545.
6 H.-R. Chen, M.-L. Su, Y.-M. Lei, Z.-X. Ye, Z.-P. Chen, P.-Y. Ma, R. Yuan, Y. Zhuo, C.-Y. Yang and W.-B. Liang, *J. Am. Chem. Soc.*, 2023, **145**, 12812–12822.
7 K. Kavita and R. R. Breaker, *Trends in Biochemical Sciences*, 2023, **48**, 119–141.
8 E. Campos-Chavez, S. Paul, Z. Zhou, D. Alonso, A. R. Verma, J. Fei and A. Mondragón, *Nat Commun*, 2024, **15**, 6592.
9 H. Salvail and R. R. Breaker, *Current Biology*, 2023, **33**, R343–R348.
10 K. Yang, N. M. Mitchell, S. Banerjee, Z. Cheng, S. Taylor, A. M. Kostic, I. Wong, S. Sajjath, Y. Zhang, J. Stevens, S. Mohan, D. W. Landry, T. S. Worgall, A. M. Andrews and M. N. Stojanovic, *Science*, 2023, **380**, 942–948.
11 S. Stangherlin, N. Lui, J. H. Lee and J. Liu, *TrAC Trends in Analytical Chemistry*, 2025, **191**, 118349.
12 L. Li, S. Xu, H. Yan, X. Li, H. S. Yazd, X. Li, T. Huang, C. Cui, J. Jiang and W. Tan, *Angew Chem Int Ed*, 2021, **60**, 2221–2231.
13 H. Yu, X. Han, W. Wang, Y. Zhang, L. Xiang, D. Bai, L. Zhang, Z. Weng, K. Lv, L. Song, W. Luo, N. Yin, Y. Zhang, T. Feng, L. Wang and G. Xie, *ACS Nano*, 2024, **18**, 12401–12411.
14 J. Xu, G. A. Wang, L. Gao, L. Wu, Q. Lei, H. Deng and F. Li, *Nat Commun*, 2023, **14**, 4248.
15 G. A. Wang, X. Wu, F. Chen, C. Shen, Q. Yang and F. Li, *J. Am. Chem. Soc.*, 2023, **145**, 2750–2753.

Chemical Science Accepted Manuscript

Please do not adjust margins

View Article Online
DOI: 10.1039/D6SC03635J

Open Access Article. Published on 02 June 2026. Downloaded on 6/3/2026 5:39:44 AM.
This article is licensed under a Creative Commons Attribution-NonCommercial 3.0 Unported Licence.

16 S. Li, P. Li, M. Ge, H. Wang, Y. Cheng, G. Li, Q. Huang, H. He, C. Cao, D. Lin and L. Yang, *Nucleic Acids Research*, 2020, **48**, 2220–2231.
17 R. C. Spitale and D. Incarnato, *Nat Rev Genet*, 2023, **24**, 178–196.
18 Y. Gao, R. Mardian, J. Ma, Y. Li, C. E. French and B. Wang, *Nat Chem Biol*, DOI:10.1038/s41589-024-01781-4.
19 R. D. Thompson, D. L. Carbaugh, J. R. Nielsen, C. M. Witt, E. M. Faison, R. M. Meganck, A. Rangadurai, B. Zhao, J. P. Bonin, N. I. Nicely, W. F. Marzluff, A. T. Frank, H. M. Lazear and Q. Zhang, *Nat Chem Biol*, DOI:10.1038/s41589-025-01843-1.
20 H. Yang, H. Tan, H. Wen, P. Xin, Y. Liu, Z. Deng, Y. Xu, F. Gao, L. Zhang, Z. Ye, Z. Zhang, Y. Chen, Y. Wang, J. Sun, J. W. Y. Lam, Z. Zhao, R. T. K. Kwok, Z. Qiu and B. Z. Tang, *ACS Nano*, 2024, **18**, 33792–33826.
21 J. Qiao, X. Xu, X. Zhou, Y. Wu, J. Wang, H. Xi, C. Liu, Y. Wang, L. Zhou, X. Zhou, H. Jiang, J. Wu, H. Deng and L. Yu, *ACS Nano*, 2025, **19**, 13037–13052.
22 Z. Weng, H. Yu, W. Luo, Y. Guo, Q. Liu, L. Zhang, Z. Zhang, T. Wang, L. Dai, X. Zhou, X. Han, L. Wang, J. Li, Y. Yang and G. Xie, *ACS Nano*, 2022, **16**, 3135–3144.
23 M. Sassanfar and J. W. Szostak, *Nature*, 1993, **364**, 550–553.
24 D. E. Huizenga and J. W. Szostak, *Biochemistry*, 1995, **34**, 656–665.
25 S. Forli, R. Huey, M. E. Pique, M. F. Sanner, D. S. Goodsell and A. J. Olson, *Nat Protoc*, 2016, **11**, 905–919.
26 O. Trott and A. J. Olson, *J Comput Chem*, 2010, **31**, 455–461.
27 J. Eberhardt, D. Santos-Martins, A. F. Tillack and S. Forli, *J. Chem. Inf. Model.*, 2021, **61**, 3891–3898.
28 Z. Chen, W. Chen, Z. Reheman, H. Jiang, J. Wu and X. Li, *Nucleic Acids Research*, 2023, **51**, 8322–8336.
29 N. I. Orlovsky, H. M. Al-Hashimi and T. G. Oas, *J. Am. Chem. Soc.*, 2020, **142**, 907–921.
30 Y. Du, S. J. Zhen, B. Li, M. Byrom, Y. S. Jiang and A. D. Ellington, *Anal. Chem.*, 2016, **88**, 2250–2257.
31 B. D. Wilson, A. A. Hariri, I. A. P. Thompson, M. Eisenstein and H. T. Soh, *Nat Commun*, 2019, **10**, 5079.
32 J. D. Munzar, A. Ng and D. Juncker, *Nat Commun*, 2018, **9**, 343.
33 E. A. Dethoff, J. Chugh, A. M. Mustoe and H. M. Al-Hashimi, *Nature*, 2012, **482**, 322–330.
34 A. D. Vogt and E. Di Cera, *Biochemistry*, 2012, **51**, 5894–5902.
35 F. C. Simmel, B. Yurke and H. R. Singh, *Chem. Rev.*, 2019, **119**, 6326–6369.
36 K. Huang, X. Chen, C. Li, Q. Song, H. Li, L. Zhu, Y. Yang and A. Ren, *Nat Chem Biol*, 2021, **17**, 1289–1295.
37 Y. Zhang, J. Wang and Y. Xiao, *Computational and Structural Biotechnology Journal*, 2020, **18**, 2416–2423.
38 T. Lu and F. Chen, *J Comput Chem*, 2012, **33**, 580–592.
39 S. Hong, X. Zhang, R. J. Lake, G. T. Pawel, Z. Guo, R. Pei and Y. Lu, *Chem. Sci.*, 2020, **11**, 713–720.
40 W. Junge and N. Nelson, *Annu. Rev. Biochem.*, 2015, **84**, 631–657.
41 Z. Zou, M. Pan, F. Mo, Q. Jiang, A. Feng, Y. Zhou, F. Wang and X. Liu, *Chem. Sci.*, 2022, **13**, 12198–12207.

Chemical Science Accepted Manuscript

Please do not adjust margins

View Article Online
DOI: 10.1039/D6SC03635J

All data supporting the findings of this study are included within the article and its Electronic Supplementary Information (ESI). Data are available from the corresponding author upon reasonable request.

Open Access Article. Published on 02 June 2026. Downloaded on 6/3/2026 5:39:44 AM.
This article is licensed under a Creative Commons Attribution-NonCommercial 3.0 Unported Licence.
Chemical Science Accepted Manuscript